Received: 23 March 2021 | Revised: 23 April 2021 | Accepted: 10 May 2021

DOI: 10.1002/ese3.925

RESEARCH ARTICLE

Energy Science & Engineering
Open Access

# Impacts of fluorine in NASICON-type materials as cathodes for aqueous zinc ion batteries

**Ziyan Liu** | **Xiaoxiao Jia** | **Guozhong Cao**

Department of Materials Science and Engineering, University of Washington, Seattle, WA, USA

**Correspondence**
Guozhong Cao, Department of Materials Science and Engineering, University of Washington, Seattle, WA 98195, USA.
Email: gzcao@uw.edu

**Funding information**
National Science Foundation, Grant/Award Number: CBET-1803256

**Abstract**

Sodium superionic conductor (NASICON)-type materials are getting more and more attention due to their high capacity and good cycling ability compared with other cathode materials in aqueous zinc ion batteries (AZIB). The present paper was to study the synthesis and electrochemical properties of two NASICON compounds of $Na_3V_2(PO_4)_3$ and $Na_3V_2(PO_4)_2F_3$ and to understand the impacts of fluorine. Both $Na_3V_2(PO_4)_3$ and $Na_3V_2(PO_4)_2F_3$ are synthesized by hydrothermal growth followed with annealing at 800°C in inert gas. With 3 mol/L $Zn(CF_3SO_3)_2$ in water as electrolyte, $Na_3V_2(PO_4)_3$ offered a high storage capacity, while $Na_3V_2(PO_4)_2F_3$ demonstrated a high discharge voltage though low storage capacity. It was also found that the storage capacity of $Na_3V_2(PO_4)_2F_3$ increases with increased cycles; however, the compound undergoes a gradual phase transition. It is discussed possible approaches to attain both high discharge voltage and large capacity with good cycling stability.

## 1 | INTRODUCTION

Aqueous zinc ion battery (AZIB) has drawn increasing attention as one of the most promising candidates of aqueous rechargeable batteries. It has high volumetric capacity of 5852 mA h $cm^{-3}$ and low standard reduction potential of −0.76 V vs standard hydrogen electrode (SHE); the zinc abundancy in earth crust is 3 times higher than lithium; Zn metal is 8 times cheaper than lithium. It is environmentally friendly and safe to use.[1-4] However, it is a great challenge to design and synthesize cathode materials with desired properties of both high capacity and great cycling stability due to the high polarization of $Zn^{2+}$, stemming from strong electrostatic interaction between zinc ion and anion lattice as well as the large hydrated zinc ions.[5]

Various cathode materials have been studied and tailored to circumvent some of the problems. For example, Prussian blue analogues possess good cycling stability but suffer from very low capacity (~30 mA h $g^{-1}$ at discharge rate of 60 mA $g^{-1}$).[6] Manganese oxides such as $MnO_2$ and α-$MnO_2$ show a high initial capacity but suffer from serious rapid capacity fading ($MnO_2$ from ~240 mA h $g^{-1}$ to 80 mA h $g^{-1}$ after 15 cycles; α-$MnO_2$ from ~130 mA h $g^{-1}$ to 80 mA h $g^{-1}$ after 15 cycles).[7-9] $V_2O_5$ has high initial capacity of ~140 mA h $g^{-1}$ but also suffered from poor capacity retaining (~80%),[10] while hydrate vanadium pentoxide with pre-inserted cations demonstrated much improved zinc ion intercalation properties and battery performances.[11]

Recently, NASICON compounds as cathode materials of AZIB have attracted increasing research interest. NASICON-type sodium vanadium phosphate $Na_3V_2(PO_4)_3$ (NVP) was first synthesized and studied in 1992, and it was proposed as an host for inserting/extracting electropositive ions.[12] $Na_3V_2(PO_4)_2F_3$ (NVPF) was investigated in 1999, and basic structure of the compound was discovered.[13] Since the ionic radius of $Zn^{2+}$ is smaller than $Na^+$, theoretically the insertion

or extraction of $Zn^{2+}$ in $Na^{+}$ compound is expected to have little obstacle. Graphene-like carbon coated NVP was first tested in AZIB and demonstrated decent capacity, though with low cycling stability of only ~74% initial capacity remained after 100 cycles.[14] On the other hand, carbon coated NVPF displayed with excellent cycling ability (~95% capacity retention over 4000 cycles).[15] However, lately structural decomposition of both NVP and NVPF cathode materials was discovered as well as the product of their decompositions, which provides another unique angle to study the NASICON cathode behavior mechanism of AZIB.[16,17] It is unclear the difference between the decomposition effect due to the presence of fluorine.

Figure 1 shows the crystal structures of NVP and NVPF. The structure of NVP is oriented in the order that one octahedral $VO_6$ is cornered by four tetrahedral $PO_4$. One $PO_4$ is connected by two $VO_6$ and Na1, while Na2 is only stationed between two $VO_6$ (2 Na2 in 18e position and 1 Na1 in 6b position). The occupancy of Na1 (0.81) site is larger than the occupancy of Na2 (0.73) site, the bond length of Na1-O (2.50 Å) is shorter than Na2-O (2.63 Å) (Table 1), and result in only Na ions in Na2 sites will be extracted and replaced by Zn ion during charging process. During charging process, two $Na^{+}$ will be replaced by one $Zn^{2+}$ to create $ZnNaV_2(PO_4)_3$ and during insertion/extraction of $Zn^{2+}$, the valence of vanadium is changing from +3 to +4.[18,19] During insertion, some extracted Na ions in electrolyte will also be intercalated back to Na2 sites.

In NVPF structure, each bi-octahedral $V_2O_8F_3$ is connected by two tetrahedral $PO_4$ and one F atom, with Na1 and Na2 sites in between layers.[20] One Na ion in Na1 site and two Na ions in Na2 site are both in 8i position; however, Na ions in Na2 (0.5) only have half the occupancy of Na1 (1). The F1 is in 4f position, F2 is in 8j position, and they are both fully occupied by fluorine. The bond length of F1-Na1 is 2.50 Å, F1-Na2 is 2.74 Å, F1-V is 2.02 Å, F2-Na1 is 2.50 Å, F2-Na2 is 2.39 Å, and F2-V is 1.88 Å (Table 2). This suggests that the fluorine atoms in F1 sites have a weaker bond than in F2 sites. Due to the structure stabilization of fluorine in NVPF, initially only one $Na^{+}$ can be extracted and replaced by $Zn^{2+}$ to form $Zn_{0.5}Na_2V_2(PO_4)_2F_3$, since $Na_2V_2(PO_4)_2F_3$ is considered as a stable structure.[21] However, it is possible for fully extraction of 2 $Na^{+}$ in Na2 sites at late charge/discharge process but will result in irreversible structure decomposition.[22] Reverse insertion of $Na^{+}$ will happen due to electrolyte $Na^{+}$ presence from previous extraction process as well.

The valence electrons of V in NVP and NVPF are both +3. Based on the electronic configuration of $V^{3+}$, it is expected to see two unpaired spins in the d orbital. The bonding environment for V in both materials is high splitting octahedral crystal structures and indicates both the spins will enter the lower $t_{2g}$ orbital.[23] Such arrangement creates a large orbital energy that can contribute to the material electronic potential. Since both $O^{2-}$ and $F^{-}$ are weak field ligands, thus their effect on splitting as well as orbital energy does not have significant difference. However, the insertion of F atoms in NVPF increases the space of the matrix, which creates three-dimensional ion transport tunnels that can facilitate kinetic movements of $Zn^{2+}$ and $Na^{+}$. At the same time, the higher electronegativity for F compare with O can induce the voltage platform that results in a larger voltage potential.[24] Unfortunately, this also means $F^{-}$ has a bigger tendency to form more stable compounds with other ions during cathode decomposition.

In this work, impacts of fluorine in NASICON-type compound cathodes on the electrochemical properties and structural evolution are studied. By using XRD, SEM, EDS, and XPS characterization, as well as galvanostatic

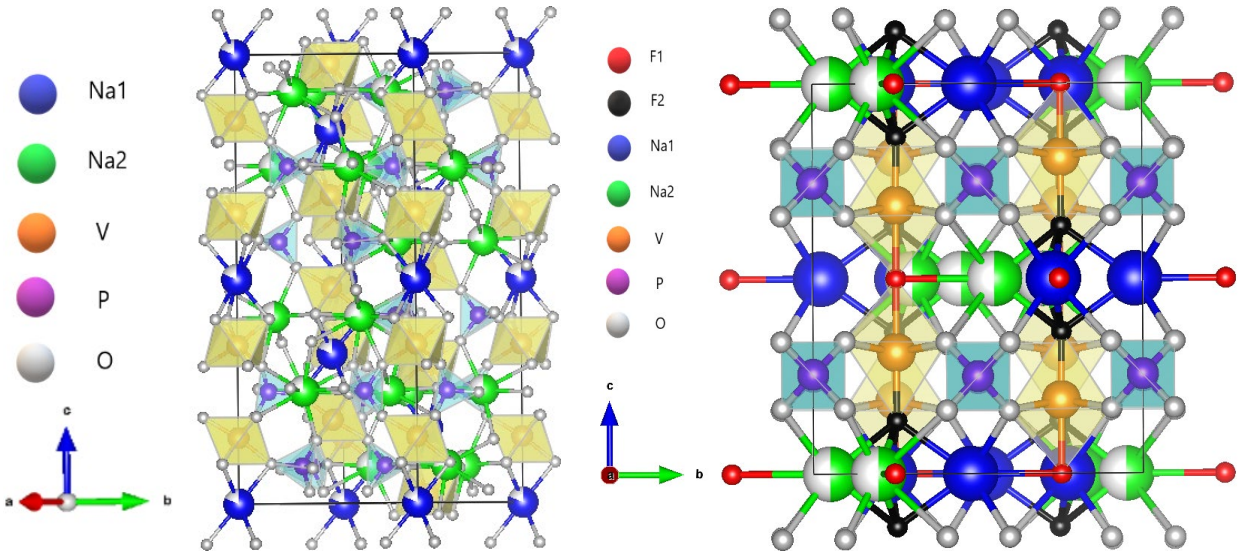


**FIGURE 1** Schematic crystal structure of NVP (left) and NVPF (right)

charge/discharge and CV tests, the hypothesis of fluorine in NASICON-type compound has significant influences on the decomposition process can be well supported. Corresponding data are analyzed, and possible mechanisms are elaborated, which may offer useful perspective on the further development and optimization of fluorine contained NASICON cathode materials.

**TABLE 1** Atomic coordination and structure parameters of NVP

| *a* | *b* | *c* | *α* | *β* | *γ* |
|---|---|---|---|---|---|
| **8.73 Å** | **8.73 Å** | **21.80 Å** | **90°** | **90°** | **120°** |
| | *x* | *y* | *z* | **Occupancy** | **Site** |
| V1 | 0.33 | 0.67 | 0.02 | 1.00 | 12c |
| Na1 | 0.33 | 0.67 | 0.17 | 0.81 | 6b |
| Na2 | 0.67 | 0.97 | 0.08 | 0.73 | 18e |
| P1 | −0.04 | 0.33 | 0.08 | 1.00 | 18e |
| O1 | 0.14 | 0.50 | 0.08 | 1.00 | 36f |
| O2 | 0.54 | 0.84 | −0.03 | 1.00 | 36f |

**TABLE 2** Atomic coordination and structure parameters of NVPF

| *a* | *b* | *c* | *α* | *β* | *γ* |
|---|---|---|---|---|---|
| **9.05 Å** | **9.05 Å** | **10.71 Å** | **90°** | **90°** | **90°** |
| | *x* | *y* | *z* | **Occupancy** | **Site** |
| F1 | 0.25 | 0.25 | 0.00 | 1.00 | 4f |
| F2 | 0.25 | 0.25 | 0.36 | 1.00 | 8j |
| Na1 | 0.52 | 0.23 | 0.00 | 1.00 | 8i |
| Na2 | 0.80 | 0.05 | 0.00 | 0.50 | 8i |
| P1 | 0.00 | 0.50 | 0.25 | 1.00 | 4d |
| P2 | 0.00 | 0.00 | 0.26 | 1.00 | 4e |
| O1 | 0.10 | 0.41 | 0.16 | 1.00 | 16k |
| O2 | 0.09 | 0.09 | 0.17 | 1.00 | 8j |
| O3 | 0.40 | 0.40 | 0.16 | 1.00 | 8j |
| V1 | 0.25 | 0.25 | 0.19 | 1.00 | 8j |

## 2 | MATERIALS AND METHODS

### 2.1 | Material synthesis

For preparing the carbon coated NVP (NVP@C), 0.48 g $Na_2CO_3$, 0.55 g $V_2O_5$, 1.05 g $NH_4H_2PO_4$, and 0.40 g ascorbic acid (as a reducing agent) were added to 75 mL distilled water under strongly stirring at 80°C. Then, 2 mL of $H_2O_2$ was added into the solution as a catalyst. Ultimately, the color of solution turned from bright orange to dark green.

For preparing the carbon coated NVPF (NVPF@C), 1.26 g NaF, 2.34 g $NH_4VO_3$, 2.30 g $NH_4H_2PO_4$, and 3.00 g citric acid (as carbon source) were added to 75 mL distilled water under strongly stirring at 80°C, until the color of solution turned from bright yellow to dark green.

Both solutions were transferred into 100 mL Teflon lined stainless steel autoclave and held at 180°C for 12 hours. Then, the obtained precipitates were washed by deionized water and freeze dried in vacuum for 2-3 days until the water was completely removed. Finally, the dry gel was grinded into fine powders and heated to 800°C for 2 hours at a heating rate of 5°C/min under Ar-5%$H_2$ gas in a tube furnace.

### 2.2 | Electrochemical property and device performance measurements

The electrochemistry of NVP@C and NVPF@C cathodes were examined in CR2032 coin cells. Cathode material

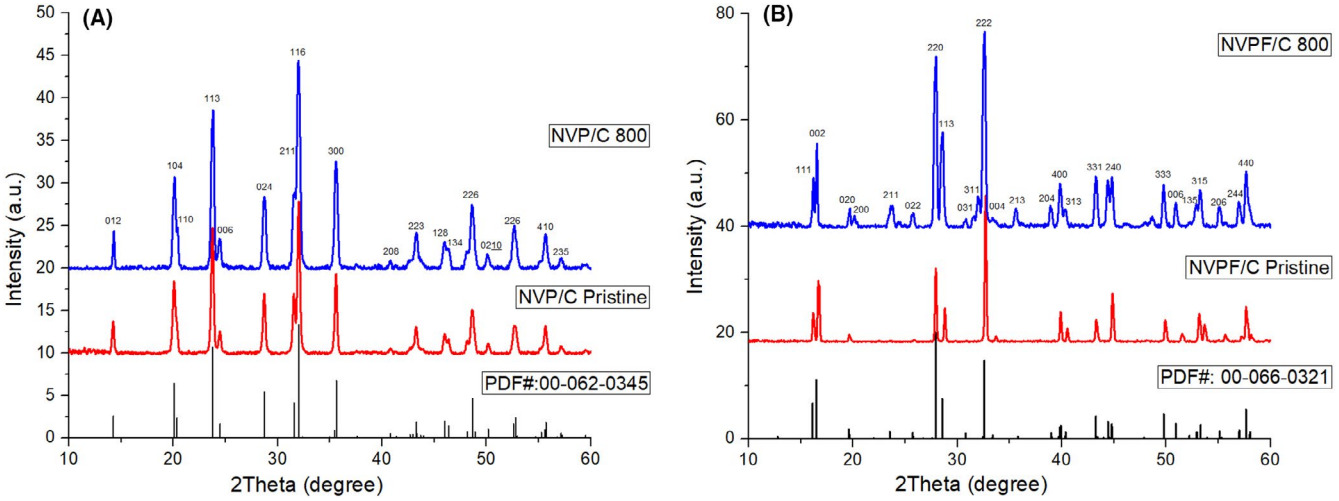


**FIGURE 2** (A) XRD patterns of pristine NVP@C and annealed at 800°C in Ar-5%$H_2$ gas for 2 h. (B) XRD of NVPF@C and annealed at 800°C in Ar-5%$H_2$ gas for 2 h

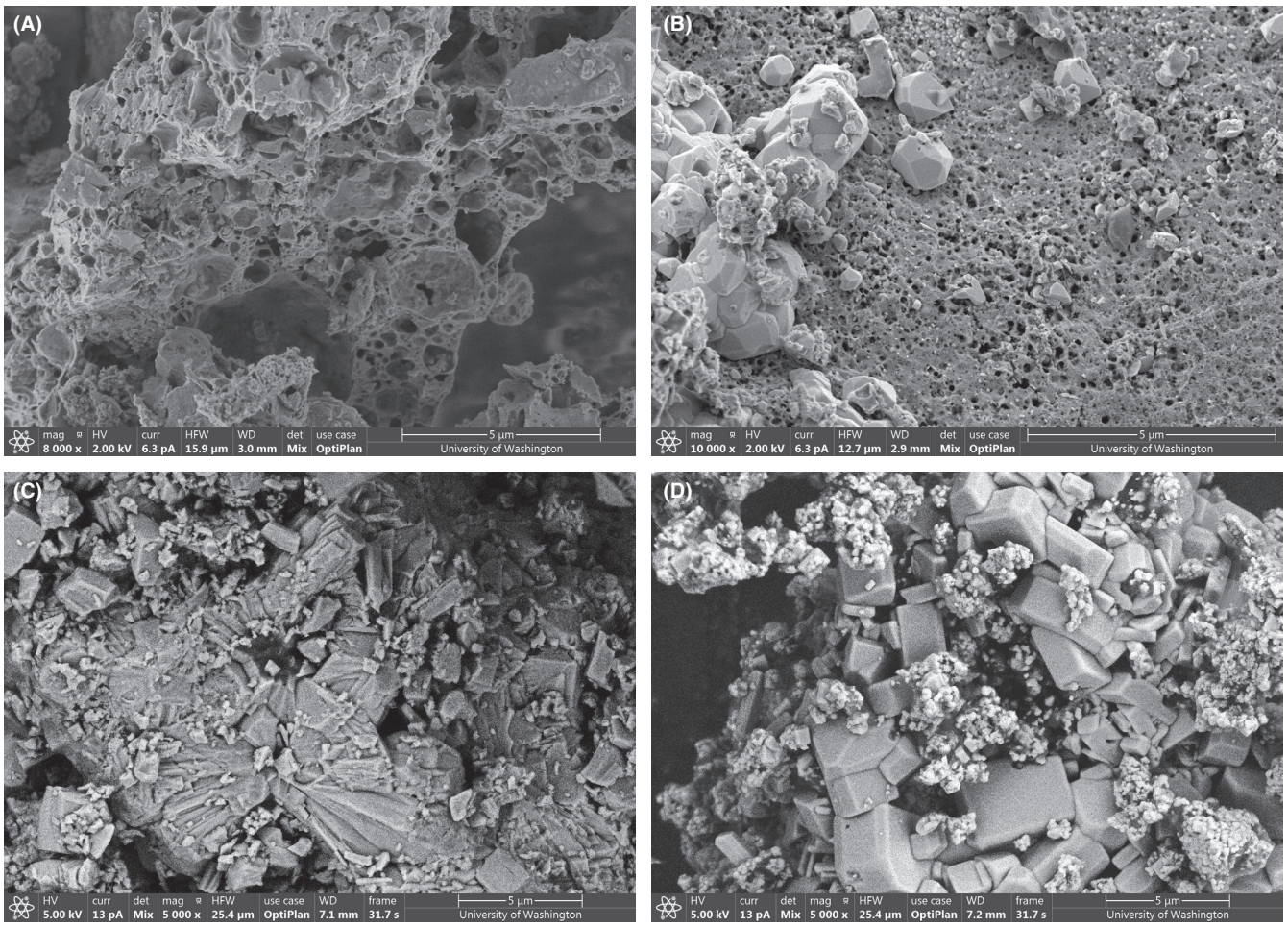


**FIGURE 3** (A) SEM image under 5 µm for pristine NVP@C. (B) SEM image under 5 µm for annealed NVP@C at 800°C. (C) SEM image under 5 µm for pristine NVPF@C. (D) SEM image under 5 µm for annealed NVPF@C at 800°C

NVP@C or NVPF@C was mixed with Super P carbon black and 20 mg/mL Polyvinylidene fluoride (PVDF) at a mass ratio of 7:2:1. The volume loading of the mixture was controlled to 0.3 mL. The mixture was then coated on ~8 mm diameter Ti disks and dried in vacuum oven at 80°C for 12 hours. Zn foil was used as the battery anode, and glass fiber was used as the separator. 3 mol/L $Zn(CF_3SO_3)_2$ was used as the aqueous electrolyte. The galvanostatic charge/discharge test was operated at a voltage range of 0.2-1.8 V with current density of 50 mA/g, and the cyclic voltammetry (CV) test was operated by a scanning rate of 0.1 mV/s at room temperature.

### 2.3 | Structural and composition characterization

The visualized models and related parameters of both NVP and NVPF crystalline structures were created by VESTA software. Crystal structures were determined by X-ray diffractometry (XRD) using a Bruker D8 Discover Microfocus XRD in 2θ from 10° to 60°. The morphologies and chemical compositions of the resulting samples were characterized by means of scanning electron microscopy (SEM) and energy-dispersive spectroscopy (EDS) using a FEI Sirion XL30 SEM. The bonding information was collected by X-ray photoelectron spectroscopy (XPS) using a Kratos Axis Ultra DLD X-ray Photoelectron Spectrometer.

## 3 | RESULTS AND DISCUSSION

Figure 2 compares XRD patterns of NVP@C and NVPF@C before and after annealing at 800°C in Ar-5%$H_2$ gas for 2 hours. All the peaks are indexed and corresponded very well to the data (PDF#: 00-062-0345 and PDF#: 00-066-0321) as well as in good agreement with literatures.[20,25-27] There is no parasitic crystalline phase detectable in all samples before and after annealing, though the enhanced intensities and reduced FWHM of XRD patterns of annealed sample suggested the annealing does improve the crystallinity and/or the growth of crystal size, in a good agreement with that reported in literature.[28] Figure 3 is the SEM pictures of NVP and NVPF before and after annealing, which revealed that particle sizes of both NVP@C and NVPF@C are larger after

annealing, corroborating the XRD results, which is in consistence with the literatures.[16,29] The surface of NVPF@C appears to be less porous and better faceted than that of NVP@C, which may attribute to the possible catalytic effects with the introduction of fluorine during the synthesis.

Figure 4A shows the CV curves of NVP@C of first three cycles at a scan rate of 0.1 mV/s from 0.2-1.8 V. There is a pair of major redox peaks observed in both electrodes. For NVP, the oxidation peak in the first cycle appears at 1.42 V corresponding to $Na^+$ extraction to form the new host ($NaV_2(PO_4)_3$). In the subsequent 2nd and 3rd cycles, redox peaks at 1.42/1.31 V are attributions of $Zn^{2+}$ intercalation/deintercalation into/from $NaV_2(PO_4)_3$, which corresponds to the valence change of $V^{3+}/V^{4+}$.[24,25] A smaller reduction peak shows around 1.05 V indicates the diffusion of Na ion from electrolyte to Na1 and Na2 sites by structural rearrangement to reduce the lattice energy, which is different from $Zn^{2+}$.[29-31] CV scan was also conducted at a scan rate of 2 mV/s with the results shown in Figure 4B. The small reduction peak disappeared. As the $Zn^{2+}$ concentration in the electrolyte is much higher than $Na^+$ and the diffusion process is more in favor of $Zn^{2+}$ intercalation during a faster discharging rate.[14,32] Figure 4C shows the CV curves of NVPF@C at 0.1 mV/s from 0.2 to 1.8 V where two pairs of redox peaks can be seen clearly. In the first cycle, the first cathodic peak at 1.37 V indicates extraction of half $Na^+$ from Na2 site to form $Na_{2\cdot5}V_2(PO_4)_2F_3$. The second peak at 1.72 V attributes to the removal of another the other half $Na^+$ in Na2 site to form $Na_2V_2(PO_4)_2F_3$ due to higher potential. The first anodic peak at 1.62 V corresponds to insertion of half $Zn^{2+}$ to form $Zn_{0.5}V_2(PO_4)_2F_3$, and the second peak at 1.21 V corresponds to sodium ion insertion. In the subsequent cycles, repeatable redox peaks at 1.37/1.21 V and 1.72/1.62 V are attributed to the stable extraction/insertion of $Na^+/Zn^{2+}$ ions, accompanied with in the valence change of vanadium ions in a mix state of $V^{3+}/V^{4+}$.[15,33] In Figure 4D, CV scans of NVP@C and

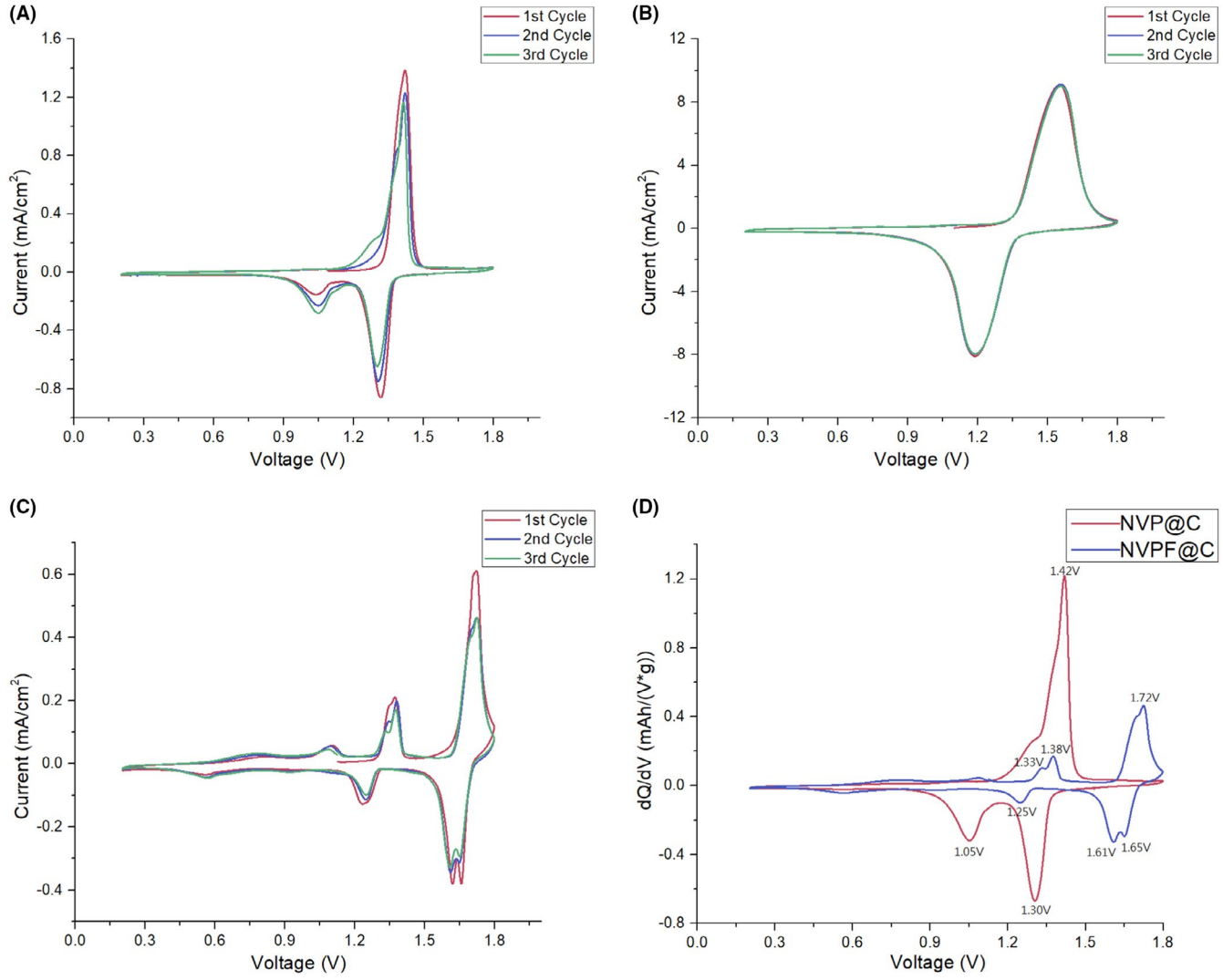


**FIGURE 4** (A) CV graph of NVP@C//Zn at a scan rate of 0.1 mV/s. (B) CV graph of NVP@C//Zn at a scan rate of 2 mV/s. (C) CV graph of NVPF@C//Zn at a scan rate of 0.1 mV/s. (D) CV scan comparison of the 3rd cycle of NVP@C and NVPF@C at a scan rate of 0.1 mV/s

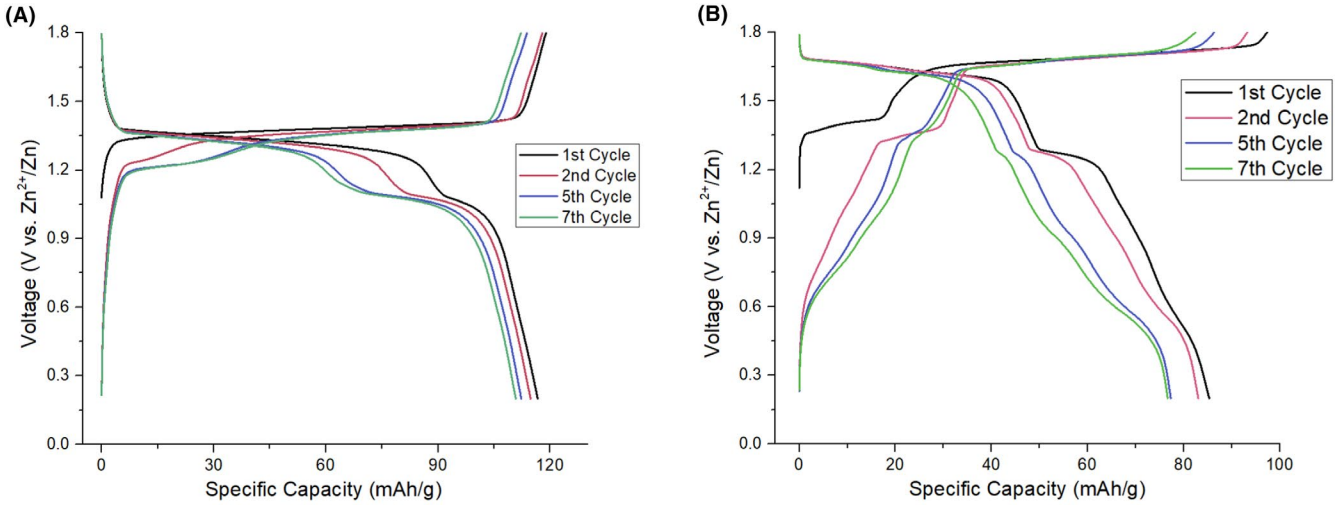


**FIGURE 5** (A) Charge and discharge curves of NVP@C//Zn at 1, 2, 5, and 7 cycles. (B) Charge and discharge curves of NVPF@C//Zn at 1, 2, 5, and 7 cycles

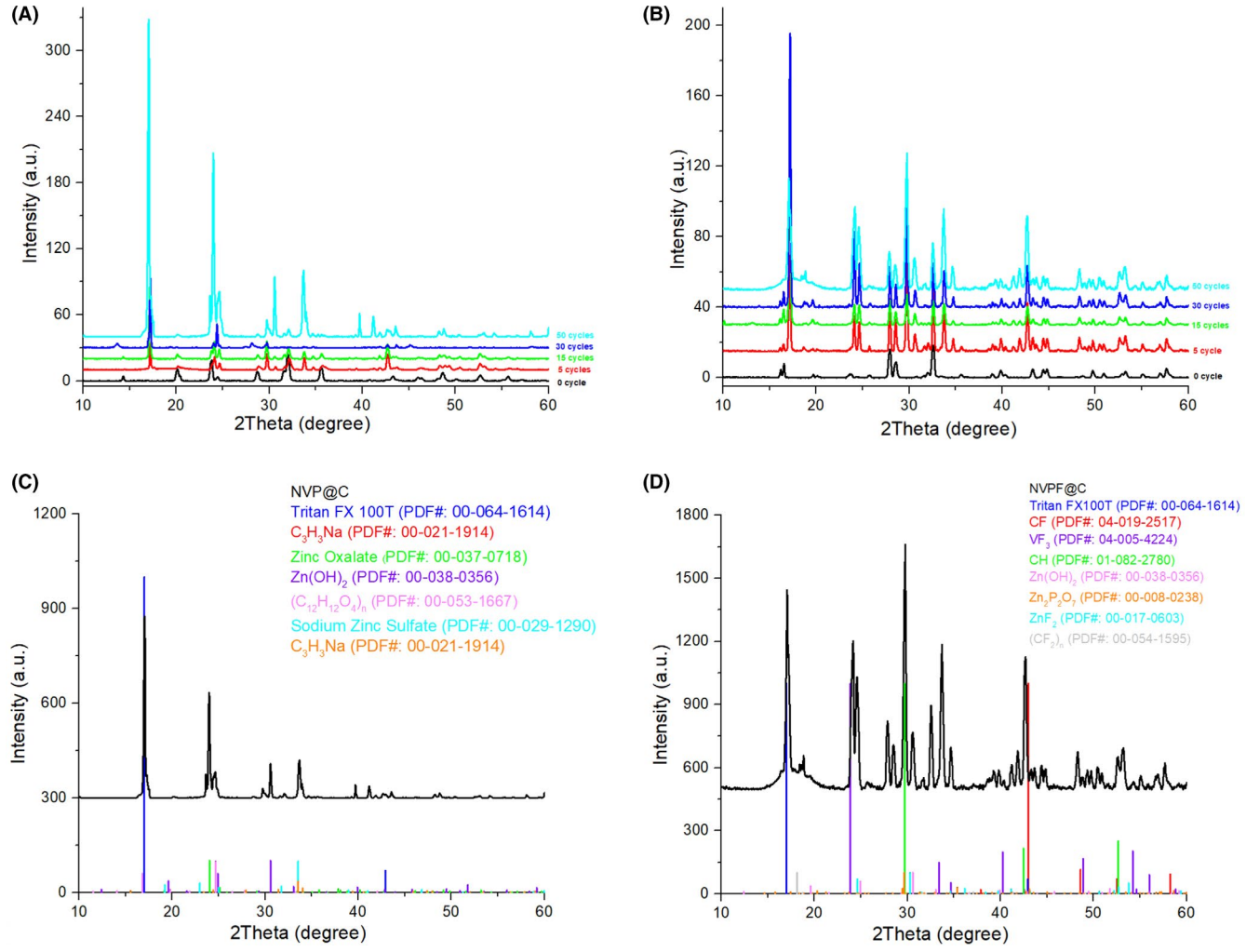


**FIGURE 6** (A) XRD patterns of NVP@C after 0, 5, 15, 30, and 50 cycles. (B) XRD patterns of NVPF@C after 0, 5, 15, 30, and 50 cycles. (C) Possible impurity phases selected by peak fitting of NVP@C surface after 50 cycles. (D) Possible impurity phases selected by peak fitting of NVPF@C surface after 50 cycles

NCPF@C at scan rate of 0.1 mV/s are compared. NVPF@C has higher redox potential with lower specific capacity compared with NVP@C. This may well attribute to the large electronegativity of fluorine, resulting in a high crystal field, the addition of fluorine can increase electronic potential as well as improve the structural stability.[21,34]

Figure 5A,B is the galvanostatic charge/discharge curves of respective NVP@C and NVPF@C cathodes at a rate of 50 mA/g. For NVP@C, there are four voltage plateaus agreeing well with two pairs of redox peaks in the corresponding CV curves. In the first cycle, only one charge plateau appears at 1.4 V attributing to the extraction of two $Na^+$ ions and the two discharge plateaus at 1.31 and 1.1 V indicate the co-insertion of $Na^+$ and $Zn^{2+}$ ions at different rates. In the second cycle, the first charge plateau appears at 1.40 V attributing to the extraction of $Na^+$ and the second charge plateau at 1.2 V corresponds to the extraction of $Zn^{2+}$. The first discharge plateau near 1.35 V is the $Zn^{2+}$ insertion and the second discharge plateau near 0.9 V indicates the $Na^+$ rearrangement.[14] For NVPF@C, the charge and discharge plateaus can be similarly attributed to the insertion/extraction of zinc and sodium ions and corroborated with the redox peaks observed in the CV curves. The first charge plateau near 1.35 V corresponding to the extraction of the first half $Na^+$ and the second charge plateau near 1.7 V indicate the extraction of the second half $Na^+$. The first discharge plateau near 1.65 V corresponding to the insertion of one half of $Zn^{2+}$ ion and the second discharge charge plateau near 1.2 V indicate the co-insertion of the $Na^+$ as proposed in literature.[15,35]

The higher charge/discharge voltages of NVPF than that of NVP are attributed to the presence of fluorine; for a give transition cation in a given crystal structure, coordination anions would affect the charge-discharge orbits by shifting the potentials level of electron accommodating d-orbitals and the potential increases with the increasing electronegativity of anions.[36] The structure has higher stability, and the movement of $Na^+$ ion is restricted which is the reason that NVPF@C has the lower initial capacity than NVP@C.[21]

Figure 6A,B shows the ex-situ XRD patterns of both NVP@C and NVPF@C after various charge-discharge cycles. After 50 cycles of charge and discharge, the intensity of original peaks is either reduced or completely disappeared. Furthermore, high intensity new peaks appeared in NVP@C at around 17°, 25°, 30°, 34°, 40°, and 42°. It is noticed that peak at around 25° cannot be fitted through the current database and may be the newly formed MVOH compounds (NaVOH/ZnVOH).[11,37] For NVPF@C, the new peaks are approximately at 16°, 25°, 30°, 35°, 42°, and 48°. By comparing both of the images, it can be seen that NVPF@C suffers more prime intensity reduction, peak shifts, background noises, and new phase formations. It indicates the decomposition phenomenon in NVPF@C is more serious than NVP@C under the same condition. In order to determine the possible products of decomposition, the XRD patterns were analyzed by peak fitting. Both results are shown in Figure 5C,D. It is noted that due to the large noise of the scan results, only the most obvious intensity peaks can be approximately determined. Also, peak shifts may be due to the broadening effect of the individual peak. The specific chemical reactions during the decomposition process are difficult to be determined; it is suspected that some of the side products may cause by reactions between the drying electrolyte and air during battery dissemble. Through the analysis, it can be seen that the presence of fluorine can be found in many impurity compounds, which indicates it might be the key element that results in serious decomposition of NVPF@C.

Figure 7A compares the CV curves of both NVP@C and NVPF@C derived from the 50th charge-discharge process.

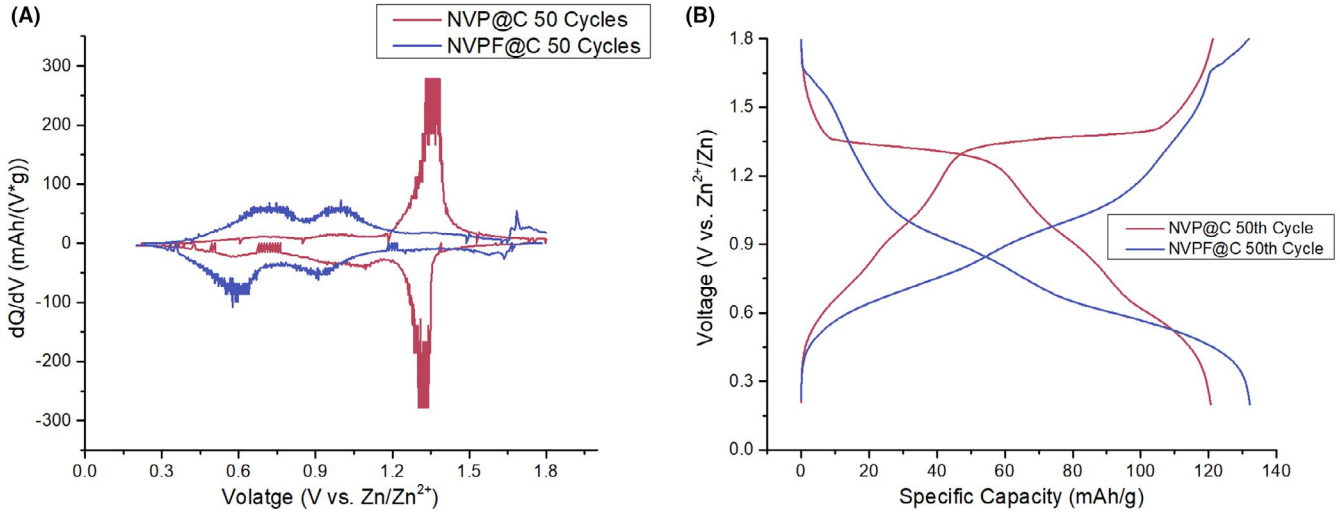


**FIGURE 7** (A) CV curves derived from galvanostatic charge/discharge tests at the 50th cycle for both NVP@C and NVPF@C. (B) Galvanostatic charge/discharge test at the 50th cycle for both NVP@C and NVPF@C

It can be seen that NVP@C retains its redox peaks with relatively strong signals at ~1.3 V. The small reduction peak at ~1.05 V disappeared, suggesting the Na ion insertion is no longer present. While in NVPF@C, the characteristic redox peaks of 1.38/1.25 V disappeared and the pair of peaks of 1.72/1.65 V possess significantly reduced intensity. Two new pairs of redox peaks appear at lower voltages of ~0.6-1.0 V, suggesting the change of electronic structure of electroactive materials. Figure 7B shows the galvanostatic charge/discharge curves of both NVP@C and NVPF@C at the 50th cycle. The new charge/discharge plateaus for NVPF@C are barely noticeable. The voltage window for NVPF@C has dropped from about 1.65 V to 0.8 V, while the voltage window for NVP@C remains almost unchanged at around 1.35 V. The much-increased capacity of NVPF@C from about 80 mAh/g to 130 mAh/g indicates the possible complete extraction of two Na ions from the matrix. The capacity does not decrease but the voltage window decreases, likely result from the phase decomposition. The exact reason for such phenomenon is still unclear; however, it is possible related to the highly conductive fluorine compounds formed during the decomposition process.

Figures 8 and 9 show the atomic compositions at surface of NVP@C and NVPF@C before and after cycling. It should be noticed that foreign elements of Ti, Si, Ca, Al, and Mg are error readings of the scan. By comparing the surface element compositions of NVP@C before and after cycling, it can be seen that the increase of O and increasing of F and S is probably due to formation of F- or O-based compounds during electrolyte or PVDF decomposition. The insertion of $Zn^{2+}$ and extraction of $Na^{+}$ cause the appearance of Zn element and decreasing of Na weight percentage. The decreasing of V and P elements indicates the occurrence of cathode decomposition. In NVPF@C, it can be seen that the cathode is also going through decomposition process; however, the increase in vanadium content could be a scanning error. The composition mapping of both cathode materials shows the change of chemical contents after cycling, and it can be seen that the decomposition behavior on NVPF@C surface is less uniform and more severe than on NVP@C.

Figure 10A shows C 1s spectra for both NVP@C and NVPF@C. After 50 cycles, the intensity of C-C/C-H (~284.8 eV) compared with pristine state is dramatically reduced. Other peaks such as aromatic C or C=O (for NVP@C)

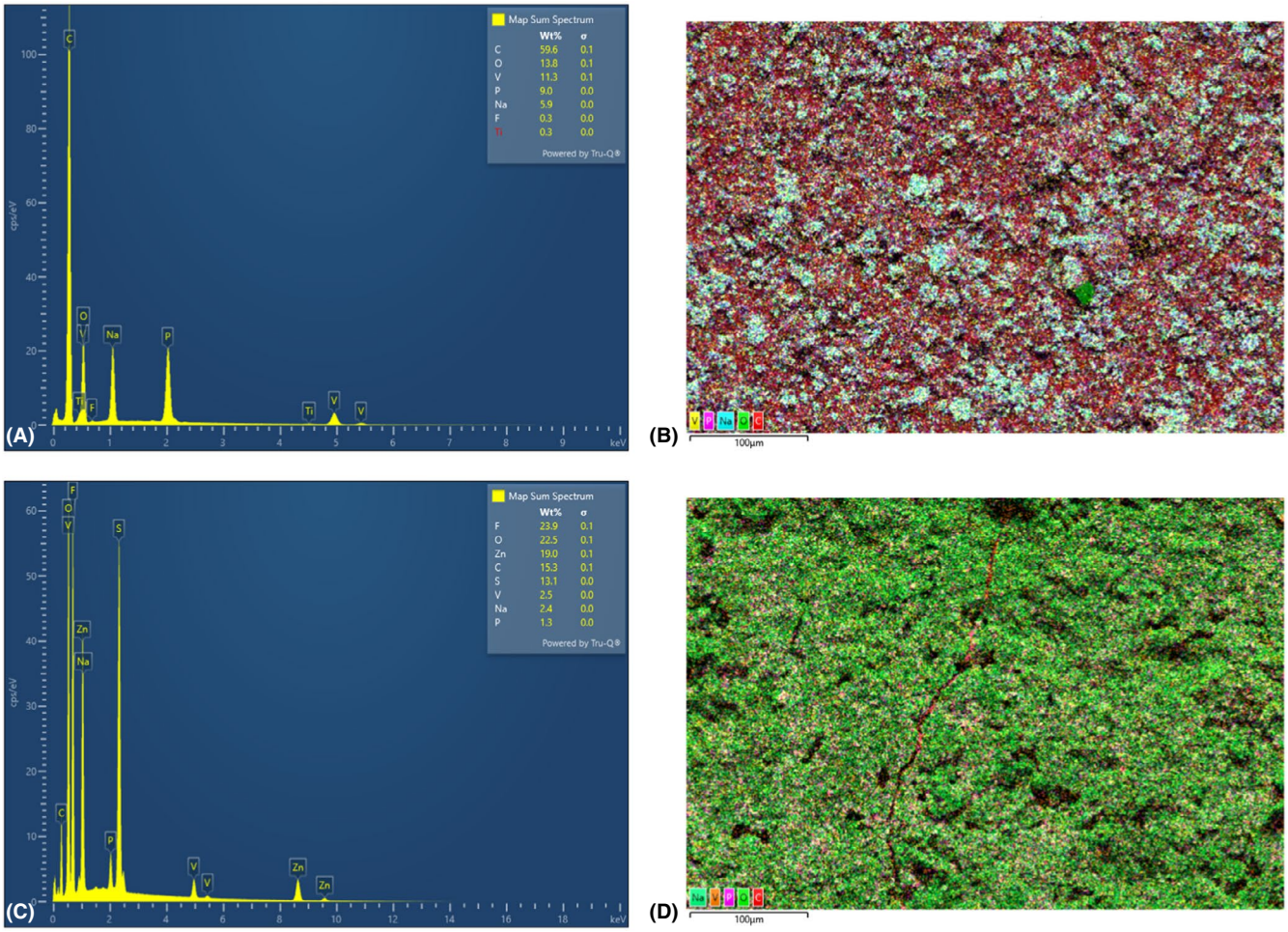


**FIGURE 8** EDS and atomic composition mapping of NVP@C (A and B) Before cycling. (C and D) After the 50th cycles

are completely disappeared. The increased intensity of C-O peaks at ~286 eV for both materials may be due to the carbon oxidation at the interface.[17] Metal-C peak newly appears at ~281 eV for NVP@C may be due to the formation of solid electrolyte interface (SEI) at the sample surface. It can also clearly see that the presence of strong C-F peaks at ~293 eV for both materials after cycling. The source of F may come from electrolyte as well as PVDF during the decomposition process. Figure 10B shows F 1s spectra in both material before and after cycle. In pristine NVP@C, C-F, and metal-F peaks at ~690 and ~688 eV may imply that F in PVDF is forming bonds with C and Na. While for pristine NVPF@C, two metal-F peaks are spotted at ~685 and ~688 eV may correspond to V-F and Na-F. After 50 cycles, both materials exhibit only one large C-F peak at ~688.5 eV; however, the broadness of the F 1s peak indicates there are more than one C-F bonding environments for both materials. Figure 10C shows V 2p spectra of both materials. For pristine NVP@C, the peak at ~517.4 and ~524.8 eV corresponds to $V^{3+}$ environment which agree with the chemical formular. However, the spectrum changes significantly after 50 cycles. The reduced intensities of $V^{3+}$ peaks indicate the material decomposed into other vanadium valance states (+4/+5).[16] The disappearance of Na peak corresponds to complete $Na^{+}$ extraction. The increasing of metal hydroxide and decreasing of metal-O indicates $H_2O$ solvation effect during decomposition. For pristine NVPF@C, the peaks at ~518 and ~525 eV indicate the corresponding $V^{3+}$ valence environment. After 50 cycles, the vanadium peaks are too low to be detected, which indicates that vanadium is almost decomposed out of the NVPF structure into other compounds.

It was found that the valence charge of ions in NVPF is slightly larger than in NVP, which makes them easier to form stable ionic compound with fluorine, especially with transition metal such as vanadium.[21,38] In addition, formation of possible SEI on NVPF@C surface was in a good agreement with literature,[15] and because of the small volume and high concentration of $Zn^{2+}$ ions,[39] $Zn^{2+}$ can penetrate the SEI and keep forming Metal-F and C-F bonds during the decomposition process. The absence of fluorine may propagate the structural collapsing of the NVPF during original cathode decomposition process. It may be predicted that such phenomenon creates a detrimental cycle until fluorine in lower energy site is depleted from the structure, which increases the speed

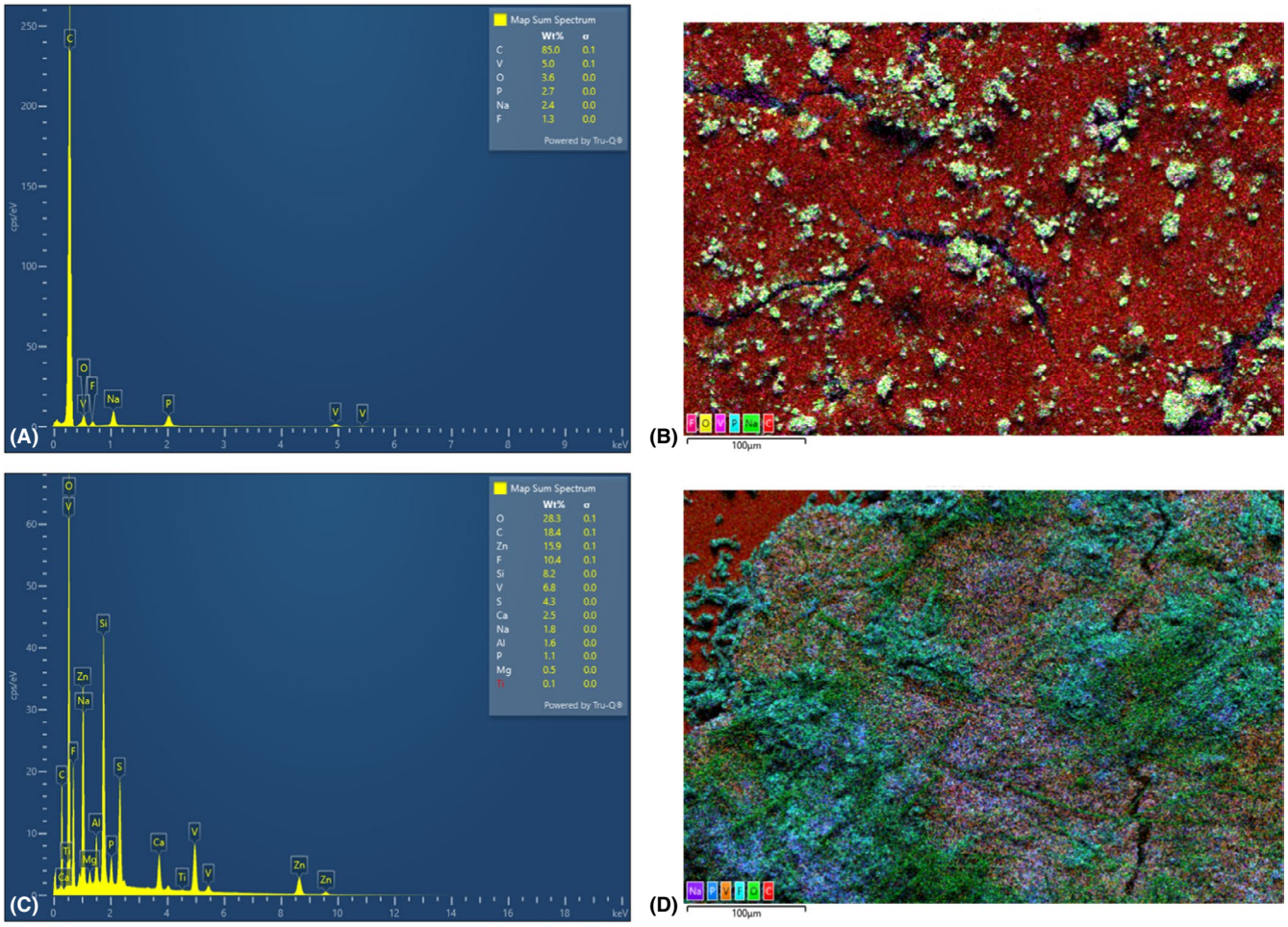


**FIGURE 9** EDS and atomic composition mapping of NVPF@C (A and B) Before cycling. (C and D) After the 50th cycles

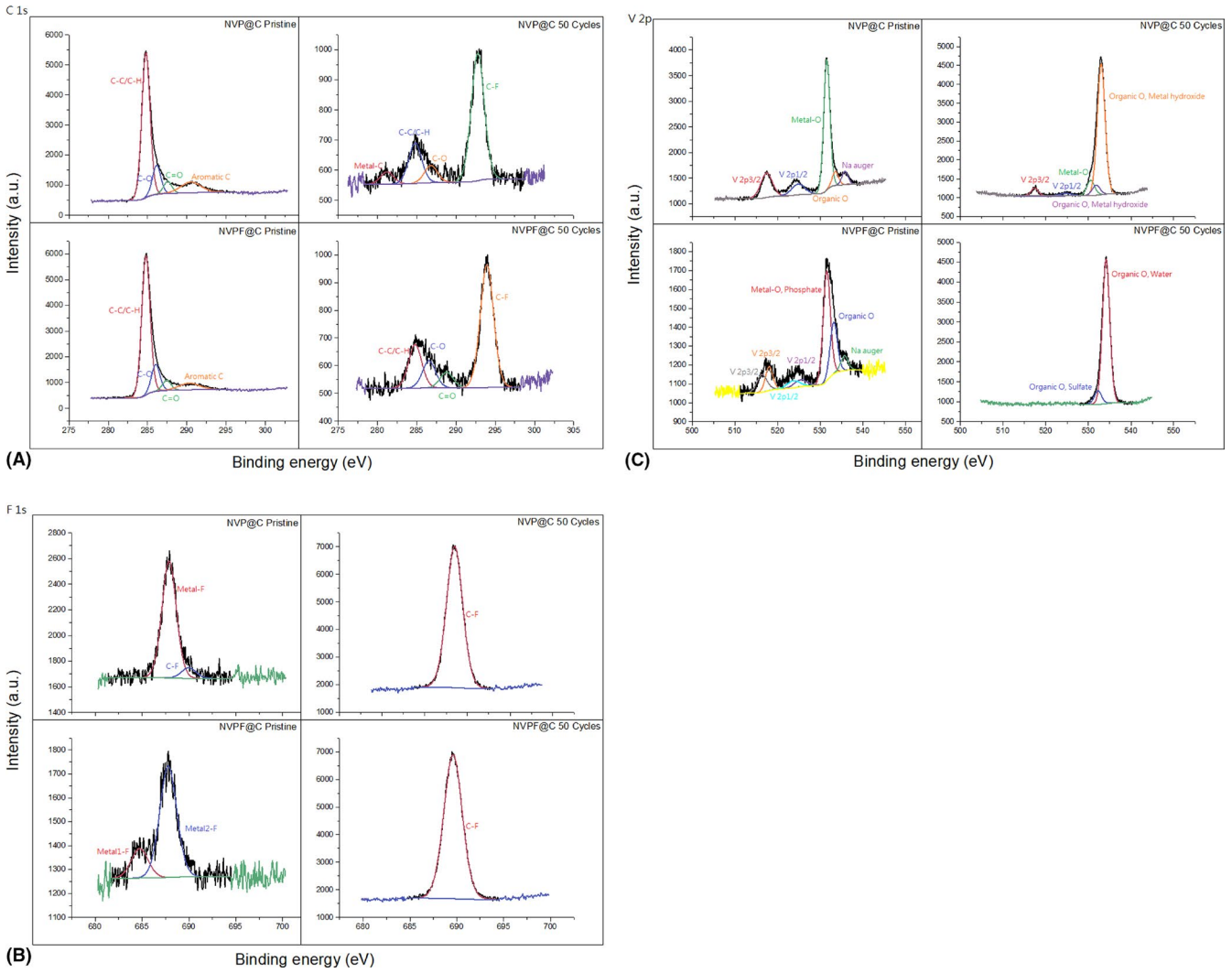


**FIGURE 10** (A) XPS C 1s spectra for NVP@C and NVPF@C in pristine and cycled state. (B) XPS F 1s spectra for NVP@C and NVPF@C in pristine and cycled state. (C) XPS V 2p spectra for NVP@C and NVPF@C in pristine and cycled state

of decomposition. By analyzing the collected data, due to all the evidence displayed, it could be reasonably concluded that the presence of fluorine is acting as a negative factor for cycle stability in NASICON-type cathodes for AZIB. To possibly suppress the fluorine reactions from NVPF with other ions, a thin protective fluorine compound layer can be coated to NVPF surface. During original cathode decomposition, the ions in the electrolyte may prioritize the protection layer for reaction, which may significantly slow down the cathode decomposition process. It is also possible to add active fluorine ions in electrolyte to achieve the same goal, which may provide a good research direction to future optimization for fluorine contained cathode materials.

## 4 | CONCLUSIONS

Carbon coated $Na_3V_2(PO_4)_3$ and $Na_3V_2(PO_4)_2F_3$ without detectable parasitic impurity phase were synthesized by hydrothermal growth followed with annealing in inert gas at 800°C and tested as cathodes in AZIBs with 3 mol/L $Zn(CF_3SO_3)_2$ aqueous electrolyte. $Na_3V_2(PO_4)_3$ demonstrated a large zinc ion storage capacity with a good cycling stability, while fluorine in $Na_3V_2(PO_4)_2F_3$ effectively enhanced the redox potential, due to its large electronegativity and its impacts on crystal field; however, it compromises the phase stability during the charge-discharge cycling, though with an increased storage capacity.

The fluorine ions with strong electronegativity are readily leached by acidic aqueous electrolyte, leading to the collapse of $Na_3V_2(PO_4)_2F_3$. Passive coating or enhanced pH value of aqueous electrolyte may retard the leach of fluorine from $Na_3V_2(PO_4)_2F_3$, which are the subjects for further study.

## ACKNOWLEDGMENTS

This work was supported by the National Science Foundation (CBET-1803256). Part of this work was conducted at the Molecular Analysis Facility (NNCI-1542101), a National Nanotechnology Coordinated Infrastructure site at the

University of Washington, which is supported in part by the National Science Foundation, the University of Washington, the Molecular Engineering & Sciences Institute, and the Clean Energy Institute. Special thanks to Samantha Young and Scott Braswell for data analysis assistance.

## CONFLICT OF INTEREST

The authors declare no source of conflict of interest.

## ORCID

*Ziyan Liu* https://orcid.org/0000-0001-9500-7894

## REFERENCES


1. Andrews JL, Banerjee S. It's not over until the big ion dances: potassium gets its groove on. *Joule*. 2018;2(11):2194-2197.
2. Wang M, Zhang F, Lee C-S, Tang Y. Low-cost metallic anode materials for high performance rechargeable batteries. *Adv Energy Mater*. 2017;7(23):1700536.
3. Tang B, Shan L, Liang S, Zhou J. Issues and opportunities facing aqueous zinc-ion batteries. *Energy Environ Sci*. 2019;12(11):3288-3304.
4. Ji B, Yao W, Tang Y. High-performance rechargeable zinc-based dual-ion batteries. *Sustain Energy Fuels*. 2020;4(1):101-107.
5. Wang L, Huang K-W, Chen J, Zheng J. Ultralong cycle stability of aqueous zinc-ion batteries with zinc vanadium oxide cathodes. *Sci Adv*. 2019;5(10):eaax4279.
6. Liu Z, Pulletikurthi G, Endres F. A Prussian blue/zinc secondary battery with a bio-ionic liquid-water mixture as electrolyte. *ACS Appl Mater Interfaces*. 2016;8(19):12158-12164.
7. Xu C, Li B, Du H, Kang F. Energetic zinc ion chemistry: the rechargeable zinc ion battery. *Angew Chem Int Ed*. 2012;51(4):933-935.
8. Pan H, Shao Y, Yan P, et al. Reversible aqueous zinc/manganese oxide energy storage from conversion reactions. *Nature Energy*. 2016;1(5):16039.
9. Zhao Y, Zhu Y, Zhang X. Challenges and perspectives for manganese-based oxides for advanced aqueous zinc-ion batteries. *InfoMat*. 2020;2(2):237-260.
10. Hu P, Yan M, Zhu T, et al. Zn/$V_2O_5$ aqueous hybrid-ion battery with high voltage platform and long cycle life. *ACS Appl Mater Interfaces*. 2017;9(49):42717-42722.
11. Liu C, Tian M, Wang M, et al. Catalyzing zinc-ion intercalation in hydrated vanadates for aqueous zinc-ion batteries. *J Mater Chem A*. 2020;8(16):7713-7723.
12. Gopalakrishnan J, Rangan KK. Vanadium phosphate ($V_2(PO_4)_3$): a novel NASICO N-type vanadium phosphate synthesized by oxidative deintercalation of sodium from sodium vanadium phosphate ($Na_3V_2(PO_4)_3$). *Chem Mater*. 1992;4(4):745-747.
13. Le Meins JM, Crosnier-Lopez MP, Hemon-Ribaud A, Courbion G. Phase transitions in the $Na_3M_2(PO_4)2F_3$ Family (M = $Al^{3+}$, $V^{3+}$, $Cr^{3+}$, $Fe^{3+}$, $Ga^{3+}$): synthesis, thermal, structural, and magnetic studies. *J Solid State Chem*. 1999;148(2):260-277.
14. Li G, Yang Z, Jiang Y, et al. Towards polyvalent ion batteries: a zinc-ion battery based on NASICON structured $Na_3V_2(PO_4)_3$. *Nano Energy*. 2016;25:211-217.
15. Li W, Wang K, Cheng S, Jiang K. A long-life aqueous Zn-ion battery based on $Na_3V_2(PO_4)2F_3$ cathode. *Energy Storage Mater*. 2018;15:14-21.
16. Li W, Jing X, Jiang K, Wang D. Observation of structural decomposition of $Na_3V_2(PO_4)_3$ and $Na_3V_2(PO_4)2F_3$ as cathodes for aqueous zn-ion batteries. *ACS Appl Energy Mater*. 2021;4(3):2797-2807. https://doi.org/10.1021/acsaem.1c00067
17. Zhang X, Ma J, Hu P, et al. An insight into failure mechanism of NASICON-structured $Na_3V_2(PO_4)_3$ in hybrid aqueous rechargeable battery. *J Energy Chem*. 2019;32:1-7.
18. Jian Z, Han W, Lu X, et al. Superior electrochemical performance and storage mechanism of $Na_3V_2(PO_4)_3$ cathode for room-temperature sodium-ion batteries. *Adv Energy Mater*. 2013;3(2):156-160.
19. Jian Z, Yuan C, Han W, et al. Atomic structure and kinetics of NASICON $Na_xV_2(PO_4)_3$ cathode for sodium-ion batteries. *Adv Func Mater*. 2014;24(27):4265-4272.
20. Shakoor RA, Seo D-H, Kim H, et al. A combined first principles and experimental study on $Na_3V_2(PO_4)2F_3$ for rechargeable Na batteries. *J Mater Chem*. 2012;22(38):20535-20541.
21. Song W, Wu Z, Chen J, et al. High-voltage NASICON sodium ion batteries: merits of fluorine insertion. *Electrochim Acta*. 2014;146:142-150.
22. Gover RKB, Bryan A, Burns P, Barker J. The electrochemical insertion properties of sodium vanadium fluorophosphate, $Na_3V_2(PO_4)2F_3$. *Solid State Ionics*. 2006;177(17):1495-1500.
23. Griffith JS, Orgel LE. Ligand-field theory. *Quart Rev Chem Soc*. 1957;11(4):381-393.
24. Wang M, Huang X, Wang H, Zhou T, Xie H, Ren Y. Synthesis and electrochemical performances of $Na_3V_2(PO_4)2F_3$/C composites as cathode materials for sodium ion batteries. *RSC Adv*. 2019;9(53):30628-30636.
25. Saravanan K, Mason CW, Rudola A, Wong KH, Balaya P. The first report on excellent cycling stability and superior rate capability of $Na_3V_2(PO_4)_3$ for sodium ion batteries. *Adv Energy Mater*. 2013;3(4):444-450.
26. Hu G, Chen P, Liu Z, et al. Synthesis and electrochemical properties of $xLiFePO_4{\cdot}(1–x)Na_3V_2(PO_4)2F_3$/C composite for lithium-ion batteries. *J Alloy Compd*. 2017;696:177-184.
27. Jian Z, Zhao L, Pan H, et al. Carbon coated $Na_3V_2(PO_4)_3$ as novel electrode material for sodium ion batteries. *Electrochem Commun*. 2012;14(1):86-89.
28. AbdulKareem SK, Ajeel SA. Effect of annealing temperatures on the structural and crystalline properties of $CaTiO_3$ powder synthesized via conventional solid-state method. *Mater Today: Proc*. 2021;42:2674-2679.
29. Ko JS, Paul PP, Wan G, et al. NASICON $Na_3V_2(PO_4)_3$ enables quasi-two-stage $Na^+$ and $Zn^{2+}$ intercalation for multivalent zinc batteries. *Chem Mater*. 2020;32(7):3028-3035.
30. Guo J-Z, Wu X-L, Wan F, Wang J, Zhang X-H, Wang R-S. A superior $Na_3V_2(PO_4)_3$-based nanocomposite enhanced by both N-doped coating carbon and graphene as the cathode for sodium-ion batteries. *Chem – Eur J*. 2015;21(48):17371-17378.
31. Huang H-B, Luo S-H, Liu C-L, et al. Double-carbon coated $Na_3V_2(PO_4)_3$ as a superior cathode material for Na-ion batteries. *Appl Surf Sci*. 2019;487:1159-1166.
32. Zhang L, Huang T, Yu A. Carbon-coated $Na_3V_2(PO_4)_3$ nanocomposite as a novel high rate cathode material for aqueous sodium ion batteries. *J Alloy Compd*. 2015;646:522-527.
33. Song W, Ji X, Wu Z, et al. Exploration of ion migration mechanism and diffusion capability for $Na_3V_2(PO_4)2F_3$ cathode utilized in rechargeable sodium-ion batteries. *J Power Sources*. 2014;256:258-263.

34. Cahard D, Bizet V. The influence of fluorine in asymmetric catalysis. *Chem Soc Rev*. 2014;43(1):135-147.
35. Matts IL, Dacek S, Pietrzak TK, Malik R, Ceder G. Explaining performance-limiting mechanisms in fluorophosphate Na-ion battery cathodes through inactive transition-metal mixing and first-principles mobility calculations. *Chem Mater*. 2015;27(17):6008-6015.
36. Liu C, Neale ZG, Cao G. Understanding electrochemical potentials of cathode materials in rechargeable batteries. *Mater Today*. 2016;19(2):109-123.
37. Tian M, Liu C, Zheng J, et al. Structural engineering of hydrated vanadium oxide cathode by K+ incorporation for high-capacity and long-cycling aqueous zinc ion batteries. *Energy Storage Materials*. 2020;29:9-16.
38. Song W, Ji X, Wu Z, et al. $Na_2FePO_4F$ cathode utilized in hybrid-ion batteries: a mechanistic exploration of ion migration and diffusion capability. *J Mater Chem A*. 2014;2(8):2571-2577.
39. Song W, Ji X, Wu Z, et al. Multifunctional dual $Na_3V_2(PO_4)2F_3$ cathode for both lithium-ion and sodium-ion batteries. *RSC Adv*. 2014;4(22):11375-11383.

**How to cite this article:** Liu Z, Jia X, Cao G. Impacts of fluorine in NASICON-type materials as cathodes for aqueous zinc ion batteries. *Energy Sci Eng*. 2021;9:938–949. https://doi.org/10.1002/ese3.925